INTERNATIONAL JOURNAL OF CLIMATOLOGY
Int. J. Climatol. **34**: 3251–3263 (2014)
Published online 21 January 2014 in Wiley Online Library
(wileyonlinelibrary.com) DOI: 10.1002/joc.3910

RMetS
Royal Meteorological Society

Anomalies, trends and variability in atmospheric fields related to hailstorms in north-eastern Spain

E. García-Ortega,[a]* L. Hermida,[a] R. Hierro,[b] A. Merino,[a] E. Gascón,[a] S. Fernández-González,[a] J. L. Sánchez[a] and L. López[a]

[a] *Atmospheric Physics Group, IMA, University of León, Spain*
[b] *Facultad de Ingeniería, Universidad Austral, Buenos Aires, Argentina*

ABSTRACT: Hailstorms have become a serious meteorological risk in mid-latitude countries because of their small-scale development and short time span, and their forecasting remains problematic. Moreover, the lack of reliable hailstorm databases is an important handicap for Numerical Weather Prediction (NWP) model validation, time trend studies and establishment of hailstorm relationships with global warming and climate change. However, this can be overcome by ascertaining physical relationships between favourable synoptic patterns and mesoscale trigger factors for hailstorm development in a local study area.

North-eastern Spain is one of the European regions with largest number of hailstorm days (HD) observed in the summer. Since 2001, from May through September, reliable databases of hailstorm occurrence in the middle Ebro Valley have been constructed, which include intensity, temporal frequency and spatial coordinate data. June and July 2006 had the largest number of HD in 2001–2010. With the objective of analysing meteorological factors responsible for this anomaly, atmospheric patterns at low and mid-tropospheric levels were studied. We determined a set of special synoptic configurations, with an evident deviation from climatic values generating anomalies of 850 hPa temperature relative to the characteristic values of 2001–2010 and 1950–2010. An analysis of these anomalies detected a positive trend of 850 hPa temperature and geopotential height in the western Mediterranean area. As a consequence, the characteristic synoptic circulation has changed since 1950, towards low-level patterns favouring adequate thermodynamic environments for hailstorm development in north-eastern Spain. Finally, after a cluster analysis, we studied periodicities in the monthly 850 hPa temperature field to improve knowledge for seasonal forecasting of hailstorms.

KEY WORDS hailstorms; western Mediterranean; anomalies; trends; Morlet transform

Received 26 June 2013; Revised 18 September 2013; Accepted 4 December 2013

1. Introduction

Hailstorms are defined as small-scale severe weather phenomena and represent one of the most important meteorological risks in mid-latitude continental areas. In the Mediterranean and south-western Europe, summer hailstorms have significant economic impacts that are not only restricted to agriculture but also affect industry and property, and occasionally cause loss of life.

Severe convection refers to the transfer of heat and humidity through vertical drafts associated with buoyancy, which can cause adverse phenomena such as hail, tornadoes, intense precipitation and strong winds. Doswell (1987) and Houze (1993) established mechanisms forming a pre-convective environment, namely atmospheric instability, low-level moisture and a trigger factor. Thermodynamic conditions favouring the onset of convection are well known. However, detection and documentation of hailstorms is very complex because of their large spatial and temporal variability and the fact that they are small-scale convective phenomena. For these reasons, observation analysis and forecasting of hailstorms present major challenges. Within these, the most important objectives are improvement of spatial and temporal precision and the availability of forecasts with sufficient lead time to minimize damage.

North-eastern Spain, specifically the middle Ebro Valley (MEV, Figure 1), is one of the areas in Europe with the greatest frequency of severe convective phenomena (Brooks *et al.*, 2003), together with the Alps and the Balkans. Storms are severe in some instances, precipitating large hail and causing major losses (García-Ortega *et al.*, 2007). Damage caused by hail is about 100 million Euros per year, which indicates that hail is not only frequent but also has important social and economic impacts. Since 2001, the Atmospheric Physics Group (GFA) at the University of León (ULE) in Spain has detected and tracked hailstorms in the MEV from May through September, using a nowcasting model with C-band radar (López and Sánchez, 2009; Sánchez *et al.*, 2013). There is also an extensive network of hailpads and volunteer observers that verify time and location of hail fall and provide relevant information, such as size

* Correspondence to: E. García-Ortega, Atmospheric Physics Group, IMA, University of León, 24071 León, Spain.
E-mail: eduardo.garcia@unileon.es

distribution or associated kinetic energy (Sánchez *et al.*, 2009). The GFA has established two objective classifications, at both synoptic scale (García-Ortega *et al.*, 2011) and mesoscale (García-Ortega *et al.*, 2012; Merino *et al.*, 2013). These define dynamic and thermodynamic environments favourable to the onset and development of convection that produces hail in the MEV.

Warming of the climate system is unequivocal, as is now evident from the observations of increasing global average temperature. In south-western Europe, the increase in surface temperature over 1970–2004 was shown to be between 1 and 2 °C (IPCC, 2007). The question arises as to whether any evidence suggests an increase in number or intensity of hailstorm events. Moreover, the lack of reliable surface observation systems is the chief obstacle to determining trends of hailstorm occurrence. Changes in such occurrence are generally difficult to quantify because they are not well captured by monitoring systems and because of historical data inhomogeneities. These facts make the question difficult to answer.

However, various studies have contributed to understanding the influence of climate change and thunderstorm and hail events. In the last few years, studies have attempted to establish a relationship between the current climatic change scenario and its consequences for intense precipitation events, hail or tornadoes, with variable results. Based on insured building damage in Germany during 1974–2003, Kunz *et al.* (2009) showed no increase in number of thunderstorm days; however, there was an increase in the number of hailstorm days (HD) and associated hail damage. In France, Berthet *et al.* (2011) detected a 70% increase in hail intensity during 1989–2009, but frequency did not change significantly. Saa *et al.* (2011) did not find a relationship between hail damage and minimum summer temperature in Spain. Nevertheless, the authors indicated the importance of the unique characteristics of landscape and topography in each area.

Other authors have tried to find evidence of changes in hail precipitation. Based on loss data of an agricultural insurance company in Switzerland (1920–1999), Schiesser (2003) reported a substantial increase in the number of hail events between 1980 and 1994. Piani *et al.* (2005) concluded that in Central Italy, a growing trend of summer hailstorm frequency has been detectable since the second half of the 1970s and will likely be static or slightly increasing in the future and more evident in spring. In Ontario, Canada, Cao (2008) identified a robust, ever-increasing frequency of severe hail events over recent decades using damage data. Brooks and Dotzek (2008) found strong variability of severe thunderstorms in the Rocky Mountains, but with no clear trend over the past 50 years. Xie *et al.* (2008) did not identify a trend of mean annual hail days in China from 1960 to the early 1980s, but a statistically significant decreasing trend afterwards. Mohr and Kunz (2013) found that the atmosphere has become more unstable over Central Europe over the last two to three decades.

There is low confidence in projections of small spatial-scale phenomena such as tornadoes and hail because competing physical processes may affect future trends and current climate models do not simulate such phenomena (IPCC, 2012) and because of poor reliability of available reference data. Leslie *et al.* (2008) showed that hailstorm severity, duration and paths were sensitive to small changes in atmospheric parameters. They indicated an increase in intensity and frequency of hailstorms through 2050 in the Sydney Basin, Australia. This conclusion contrasts with the modelling study of Niall and Walsh (2005) for south-eastern Australia. In Europe, Botzen *et al.* (2010) showed that projected climate change may increase damage from hailstorms in the Netherlands. Damage is expected to be particularly huge in climate change scenarios in which global temperatures are expected to increase as much as 2 °C by 2050. Specific results for expected changes in precipitation under increased greenhouse gas emissions in Europe using regional climate models (RCMs) may be found in Tapiador and Sánchez (2008) and Tapiador (2010).

To overcome the lack of observations, relationships between hailstorm occurrence and synoptic/mesoscale atmospheric patterns can be established. Observed trends or anomalies of atmospheric conditions influence hailstorm occurrence and intensity. An understanding of connections between synoptic pattern trends and their effects on formation of local thermodynamic regimes would improve the quality of seasonal forecasts.

Based on this idea, this work focused on two main objectives. The first is to explain meteorological anomalies influencing the thermodynamic state of the atmosphere that caused an exceptional number of HD in June and July 2006 compared to 2001–2010. In view of anomalies found between 2006 atmospheric patterns and those of 2001–2010 and 1950–2010, the second objective is to investigate a significant trend in temporal evolution of representative variables that facilitate conclusions regarding trends and periodicities of hail fall in south-western Europe.

This paper is organized as follows. In Section 2, we present the methodology and databases. In Section 3, we examine and discuss results concerning atmospheric patterns, anomalies, trends and their significance, decadal rates of change and periodicities of selected fields. Section 4 gives the conclusions.

2. Methodology and databases

A high-temporal resolution C-band radar from the GFA was deployed 10 km southwest of the city of Zaragoza. This radar permits tracking and study of the spatiotemporal development of hailstorms in a radius of about 140 km (Figure 1) at sample volume resolution $1 \times 1 \times 1\,\mathrm{km}^3$. Twelve elevation angles were used, and information updates were made every 3.5 min. The short lifetime of hail events and local coverage make detection and study of hailstorms very difficult (Smith and Waldvogel, 1989).

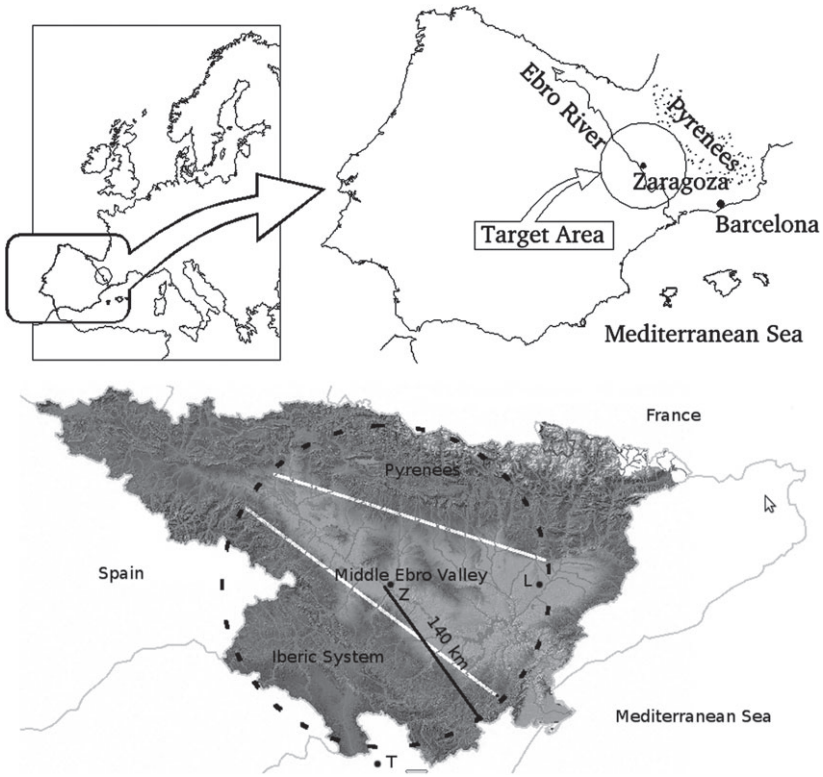

Figure 1. Study area.

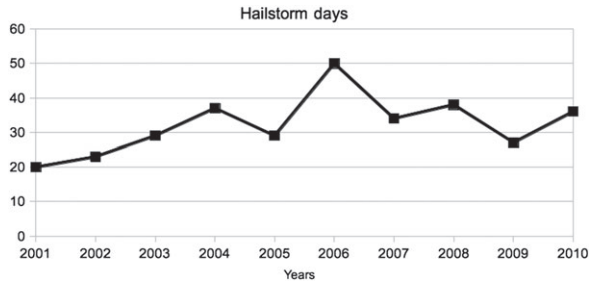

Figure 2. Time evolution of HD in MEV from 2001 to 2010.

Table 1. Monthly distribution of HD in MEV for 2001–2010.

	May	June	July	August	September	Total
2001	1	0	9	6	4	20
2002	2	4	7	6	4	23
2003	2	6	10	10	1	29
2004	2	6	11	14	4	37
2005	1	10	5	8	5	29
2006	5	17	16	4	8	50
2007	7	8	6	9	4	34
2008	6	6	11	15	1	39
2009	6	6	5	9	1	27
2010	1	9	10	10	6	36

For this reason, the GFA also has a network of 729 observers in the study area. Their information, together with model outputs, has provided knowledge of hailstorm number, intensity, evolution, structure and spatial distribution over 2001–2010.

The annual distribution of HD over 2001–2010 is shown in Figure 2. The maximum number was 50 in 2006, whereas the average is 32.6 days. The period analysed each year is May through September. Throughout this period, there is important climatic variability that leads to notable variations in temperature at mid-latitudes. These variations affect the intensity of troughs and ridges, as well as the intensity and extents of cold and warm air masses. For this reason, the data were stratified by month for each year of the study. The results are shown in Table 1.

The table shows that in June and July 2006, more than half the days were HD. This anomaly prompted us to study the atmospheric characteristics of those months and to compare them with representative values from 2001 to 2010 (with registered HD data) and from 1950 to 2010 to discover possible trends.

Atmospheric conditions in the study area were characterized by monthly 1950–2010 gridded reanalysis data from the National Centers for Environmental Prediction (NCEP), with latitude–longitude resolution $2.5^\circ \times 2.5^\circ$ (Kalnay *et al.*, 1996). The area is from 30°N to 50°N and 20°W to 10°E, covering south-western Europe, north-western Africa (western Mediterranean area) and the mid-latitude eastern Atlantic Ocean. This area was selected in an effort to be consistent with the study objectives and to avoid the influence of circulation features outside the area. The dynamic and thermodynamic state of the atmosphere was described by the temperature and geopotential height at 850 and 500 hPa (T850, T500, G850

and G500). These fields provide relevant information on the atmospheric state at low and mid-tropospheric levels.

We calculated anomalies of T850 for 2001–2010 and 1950–2010 in June and July. From the results, we obtained the T850 and G850 trends on a cell-by-cell basis using the Mann–Kendall test, as well as their significance. This test allows statistical determination whether the values of a variable increase or decrease over time. Rate of change in the variables was determined using the Sen method, a non-parametric estimator of trend magnitude that is robust to outliers (Sen, 1968). The calculations were done using the MAKESENS application from the Finnish Meteorological Institute (Salmi *et al.*, 2002). The slope obtained by the Sen method at each matrix point was used to estimate decadal rates of change (Beier *et al.*, 2012).

Once the trends were obtained and the T850 (not shown) and G850 fields for 1950–2010 were examined, a cluster analysis (CA) was performed with the original values of T850 as a useful means of objectively organizing the patterns into groups. Using years as variables and grid points as cases, the CA facilitated establishment of grouping structures in the matrix for the selected atmospheric fields. The non-hierarchical k-means method (Anderberg, 1973) was used, and the Euclidean distance was taken as the similarity index. Gong and Richman (1995) showed that non-hierarchical methods outperformed the hierarchical ones. Nevertheless, the decision regarding the number of groups is not a completely objective task; some subjectivity is present, based on physical evidences. Spatial structure of the decadal rates of change in temperature and geopotential height is a correct reference for providing a physical interpretation of the CA results and selecting the most appropriate number of clusters.

With the objective of studying potential periodicities present in the T850 field and using the CA results, we did a wavelet analysis. Continuous Wavelet Transform (CWT) analysis is a powerful tool for studying multiscale and non-stationary processes occurring over finite spatial and temporal domains (Lau and Weng, 1995). This technique implies a substantial advantage over the Fourier transform, in which analysis is limited to stationary signals and implies a loss of information in the temporal domain. CWT operates by translating and dilating a mother wavelet across a spatial or temporal series, obtaining the so-called continuous wavelet coefficient, from which the wavelet power spectrum can be computed. The mother wavelets, together with the continuous and discrete wavelet transforms, define the theory of wavelets (Sang, 2013).

Wang and Lu (2010) demonstrated from modelled data at different scales how to use the 2D CWT to conduct scale decomposition, field reconstruction, feature localization and directional signal search. Later, Partal (2012) showed the multi-variability of runoff regime and precipitation in the Aegean region. More recently, Li *et al.* (2013) applied a CWT analysis and wavelet variance to rainfall in Beijing and found periodic events affecting the trend of annual total precipitation series from 1724 to 2009. Heidinger *et al.* (2012) performed a wavelet multiresolution analysis to incorporate fluctuations from rain gauge signals into a trend derived from Tropical Rainfall Measuring Mission (TRMM) estimates. CWT has also been used to analyse RCM outputs to provide consistent climatologies (Tapiador *et al.*, 2011).

The Morlet wavelet is one of the most commonly used mother wavelets. Its development began with Morlet (1983) and since then different applications in the field of earth sciences have been discovered (Labat, 2005). The Morlet wavelet has been used as a non-orthogonal and complex mother wavelet, which consists of a flat wave modified by a Gaussian envelope. The wavelet function ψ_0 depends on a time variable η with zero mean and localized in time–frequency space (Torrence and Compo, 1998). This function is defined as

$$\psi_0(\eta) = \pi^{-1/4} e^{i\omega_0\eta} e^{-\eta^2/2} \tag{1}$$

where ω_0 is the non-dimensional frequency with a value of 6, which satisfies the admissibility condition (Farge, 1992). By scaling and shifting this wavelet function along the signal $f(\eta)$, the wavelet coefficients C are obtained. If s is the scale and p is the position, then

$$C(s,p) = \int_{+\infty}^{-\infty} f(\eta)\, \psi_0(s,p,\eta)\, d\eta \tag{2}$$

The wavelet coefficients represent how closely $f(\eta)$ is correlated with ψ_0 (Torrence and Compo, 1998). The wavelet analysis permits study of time series variability, considering the temporal dimension and reaching a compromise in localization of a signal in time–frequency space.

3. Results

3.1. Synoptic patterns

Figure 3 shows the geopotential height maps at 850 hPa. During 1950–2010, June and July patterns were similar, characterized by flow from the west and a small wave over the Iberian Peninsula (IP). To the west was the Azores high and to the east a high-pressure centre over eastern Algeria. However, the wave became deeper during 2001–2010, causing a trough over the western IP. In 2006, this trough was well defined with an axis west of Portugal, leading to an embedded low in June to the southwest of the IP. These patterns altered the low-level wind over north-east Spain, with a southerly component that transported warm and humid air from the Mediterranean Sea.

The 1950–2010 average pattern at 500 hPa (Figure 4) was characterized by a zonal flow with a weak wave forced by a high-pressure centre north of Africa. The configuration in 2001–2010 was similar, although geopotential values over the IP were slightly higher.

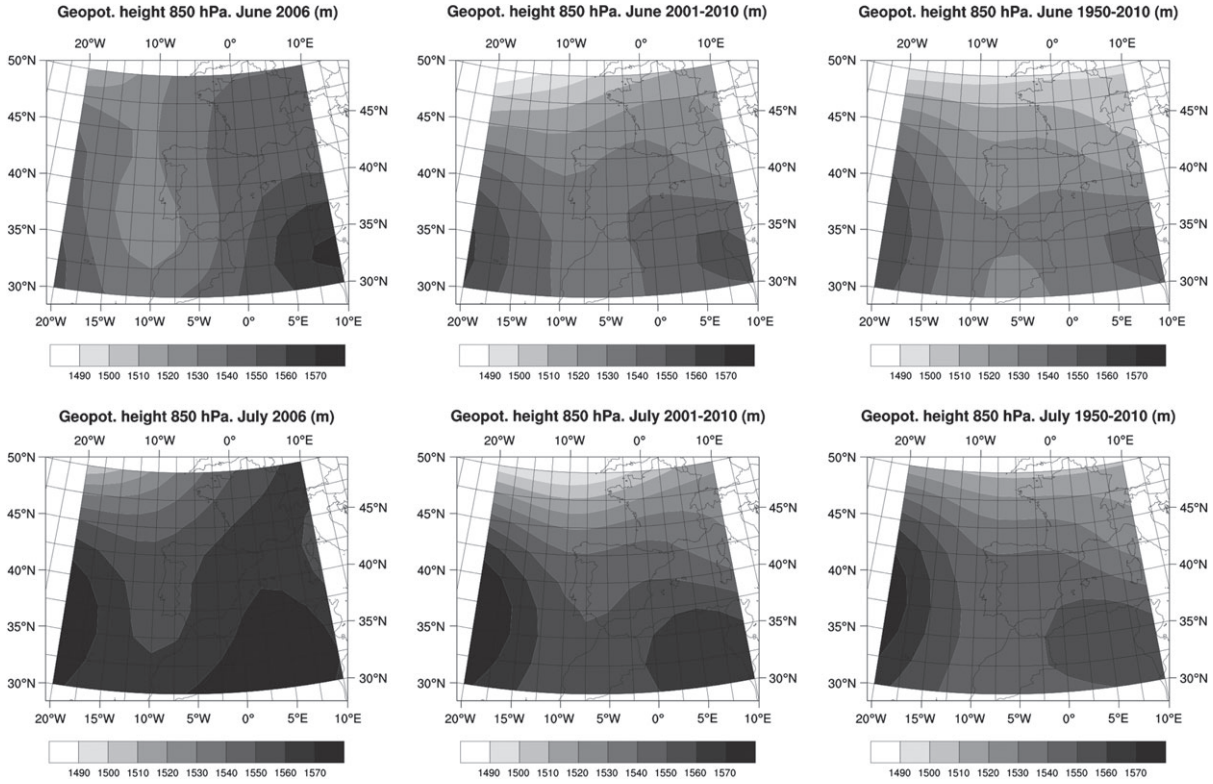

Figure 3. From left to right: geopotential height at 850 hPa in 2006; geopotential height average of 2001–2010 and of 1950–2010 (top: June, bottom: July).

However, 2006 had a trough that penetrated the western IP as an extension of that observed at 850 hPa.

The patterns observed in 2006 created favourable synoptic conditions for the formation of hailstorms in the MEV, according to the cluster classification of García-Ortega *et al.* (2011). These synoptic patterns are associated with the entrance of cold fronts that cause atmospheric instability and resulting storm formation, which are sometimes prefrontal. The presence of a trough with or without an embedded low at 850 hPa is a common characteristic in hail-risk situations in the MEV. This synoptic pattern always appears to the southwest of the study area.

The temperature field is associated with geopotential height. The presence of troughs or lows is related to the entrance of cold air masses. If these air masses are deep, they provoke unstable situations. Further, high temperatures during summer in the MEV favour the formation of thermal mesolows (Tudurí *et al.*, 2003; García-Ortega *et al.*, 2007). These mesolows, together with an appropriate low-level wind pattern, may lead to one of two phenomena. The first is formation of areas with strong convective instability, and the second is the appearance of convergence areas. Both factors are the principal ingredients for triggering convection associated with hail events (García-Ortega *et al.*, 2012). Figure 5 shows differences in temperature at 850 hPa with respect to the two studied series. From these, there was an evident increase of temperature in June and July 2006 that affected especially north-east Spain, although the geometry of the isotherms is different. In June, the area with maximum positive differences for 1950–2010 (2.5–3.0 °C) covered the north and east of the peninsula. In July, the maximum positive differences were centred over France, with 2.0–3.5 °C over the north-east Spain.

3.2. Anomalies in June and July 2006

Given the importance of the temperature difference between low and mid-tropospheric levels in the onset of convection, anomalies were calculated for the temperature difference at 850 and 500 hPa, using the standardized matrix data. For each grid point in the domain, the average value $\overline{x}$ and standard deviation σ were determined. Values outside the interval defined by $\overline{x} \pm \sigma$ were considered significant anomalies.

Positive anomalies are shown for June and July 2006 in 2001–2010 (Figure 6, left). In June, there was an anomaly in the Mediterranean, with maximum values of 2.8–3.2 °C over the island of Sardinia. Over the Atlantic to the north-west of Spain, there was also an anomaly of 0.8–1.2 °C. For 1950–2010, the anomaly was more pronounced, covering the eastern IP (1.6–2.4 °C) and extending towards the Mediterranean Sea (maxima of 3.6–4.0 °C) and Atlantic Ocean (Figure 6, top right). In both cases, the anomalies were caused by an increase in temperature at 850 hPa over the Mediterranean and to the north of the IP.

During July 2006, anomalies were observed for both series centred in south-western France (maximum values of 3.2–3.6 °C), affecting almost all the IP, with values

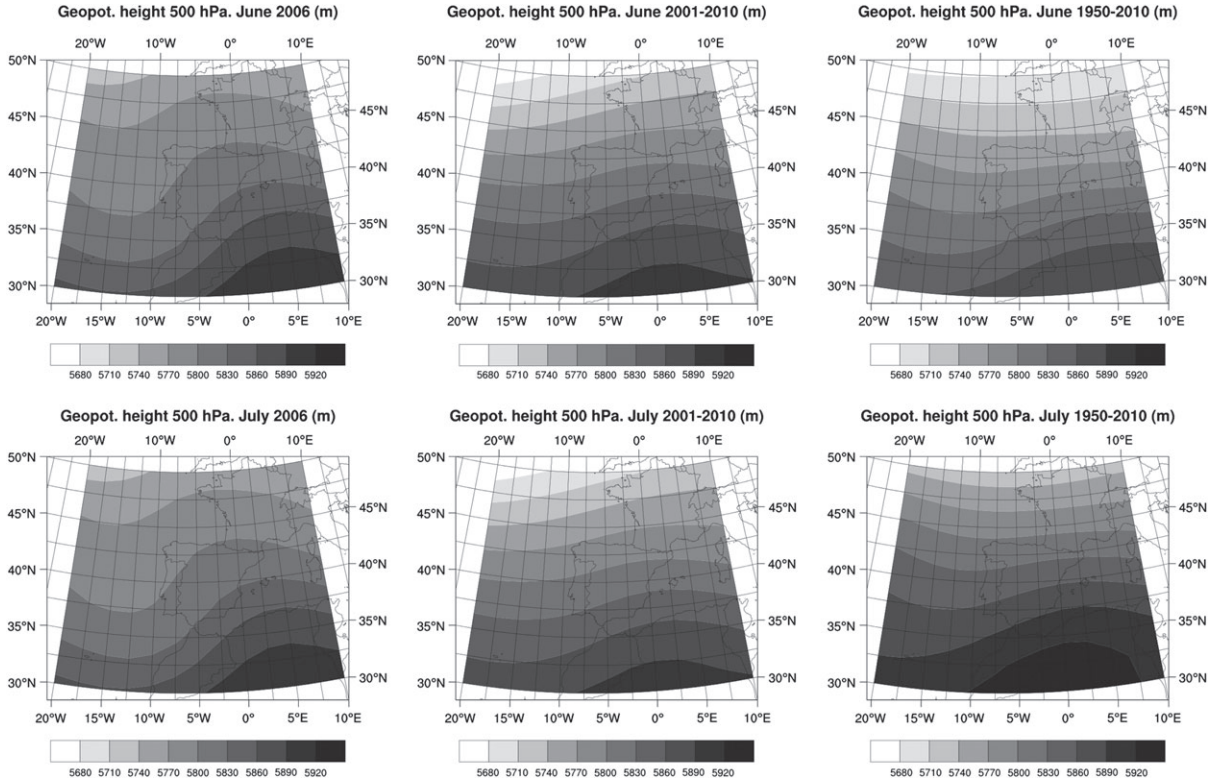

Figure 4. From left to right: geopotential height at 500 hPa in 2006, geopotential height average of 2001–2010 and of 1950–2010 (top: June, bottom: July).

of 2.0–2.8 °C in the MEV. The anomaly for 1950–2010 extended over south-eastern IP, reaching North Africa.

These anomalies were mainly due to the observed increase in T850. There were no significant differences of T500 values for either period (not shown). If differences similar to those at 850 hPa had been observed, the difference in temperature between low and mid-levels would not provide any relevant information. Another noteworthy finding is that more intense anomalies of T850 were observed for 1950–2010 than for 2001–2010. These results suggest a possible up-trend of T850 in the study area.

3.3. Trends and cluster classification for 1950–2010

We obtained T850 and G850 trends and their significance levels for 1950–2010, using the Mann–Kendall test. Figures 7 and 8 show the decadal rate of change obtained by the Sen method and the level of significance obtained from the Mann–Kendall test. Except for some grid points with slight negative trends, there was a positive decadal rate of change in T850 over nearly the entire study area. This affected the entire IP, with maximum values in the western Mediterranean and the coast of south-eastern Spain. In these areas, values exceeded 0.5 °C per decade and 0.4 °C per decade in June and July, respectively (Figure 7), with significance level $\alpha \leq 0.001$. G850 (Figure 8) showed positive decadal rate of change in both months as well. Maximum values were over the eastern study area, at 6 m per decade (June) and 5 m per decade (July). The level of significance is generally lower in areas affected by the maximum decadal rates of change ($1-\alpha > 0.95$).

A positive T850 trend was evident for 1950–2010 in the Mediterranean area near the coast of Spain. This increase was originated from strengthening of the African ridge in June and July, as shown in Figure 8. As a consequence of this strengthening, a double effect is produced: the cited increase in temperature at 850 hPa to the southeast of Spain, especially during June, which was as much as 3 °C during 1950–2010, and a wind pattern associated with strengthening of the African ridge. The increase in temperature affects the lower troposphere in the area over the Mediterranean Sea. This increases the water vapour content there. The wind pattern associated with the perturbation at G850 reinforces the southerly component of low-level wind in the area, favouring humid and warm air advection from the Mediterranean Sea to the east of the IP. This wind pattern, along with orographic characteristics of the study area, facilitates formation and development of convection in the MEV (García-Ortega *et al.*, 2012).

Thus, a reinforcement of this structure in 1950–2010 may have increased the frequency of HD in the MEV. The absence of reliable data about hail in the second half of the 20th century does not allow us to ascertain the actual temporal evolution of the number of HD since 1950. However, the present results permit affirmation of a positive trend in T850 and G850, towards patterns that generate favourable environments for hailstorm development in north-east Spain. The results are consistent with

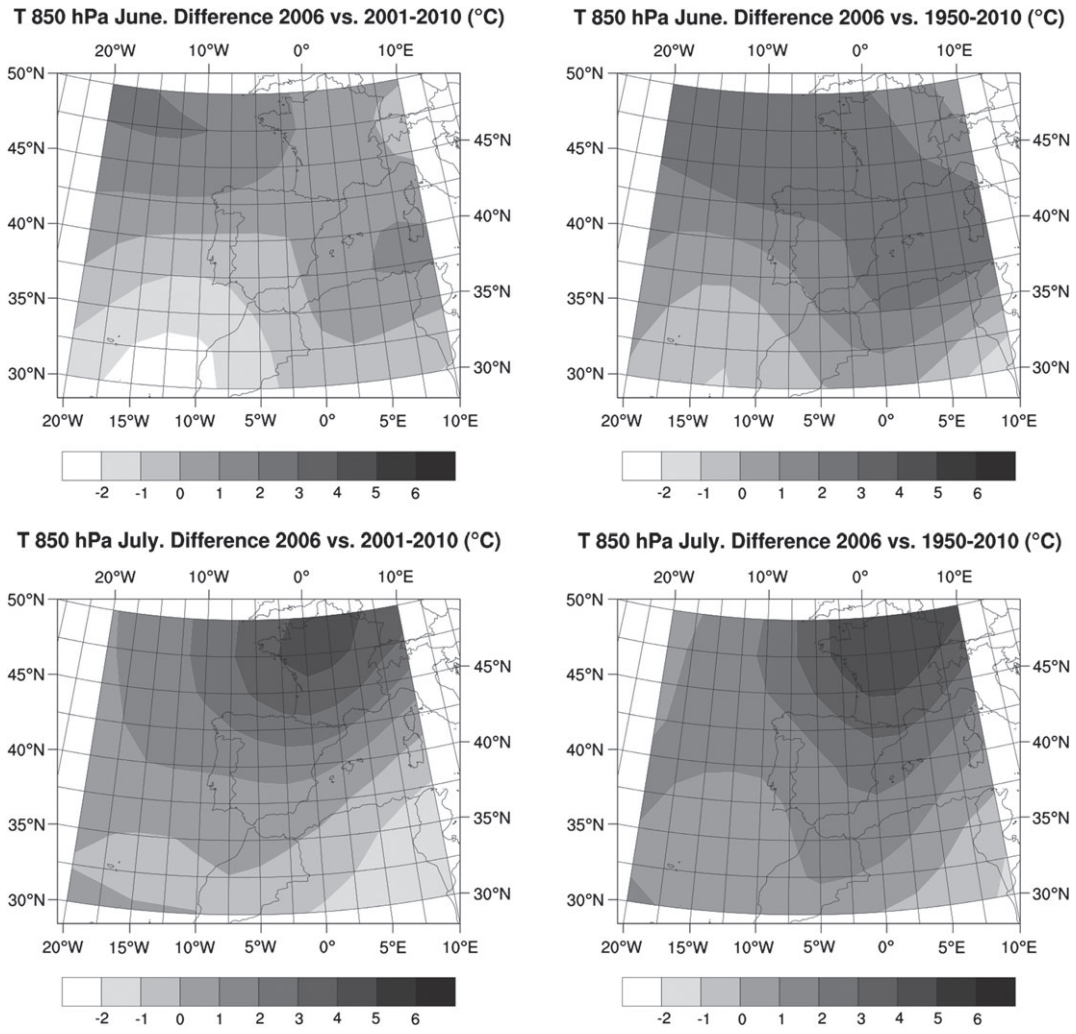

Figure 5. From left to right: 850 hPa temperature difference between 2006 and 2001–2010 average; between 2006 and 1950–2010 average (top: June, bottom: July).

the observation that the anomalies of 2006 are greater relative to 1950–2010 than to 2001–2010. Therefore, the anomaly of 2006 is an extreme case of this evolution pattern.

After confirming the T850-positive trend over the western Mediterranean Sea, the possible periodicities were studied. However, before doing that, groups that can be established between grid points were analysed, taking the T850 time series. To do this, a CA was performed for the original T850 data, using the method previously described. Based on the similarity criterion and identification of clusters with structures observed in the decadal rate changes, and the T850 patterns in 1950–2010 (not shown), two clusters were selected for both June and July (Figure 9). From this result, and taking each cluster individually, we studied periodicities within the T850 time series.

3.4. Wavelet analysis

As explained in Section 2, wavelet analysis facilitates study of temporal variability of the time series. With the objective of studying periodicities in cluster average temperature in June and July from 1950 to 2010, a CWT was applied. Although linear tendencies do not affect CWT results, the original time series were detrended because temperature data are composed of a linear trend, periods and random signal, as indicated by Yi and Shu (2012).

Figure 10 shows the CWT results, along with time series for each case. In cluster 1 of June, one mode of about 20 years appeared to persist for the entire period. Another cycle of 7 years is evident, but after 1980, an abrupt change in frequency gives way to an oscillation mode of about 8–9 years, which persists the remaining time. One can detect the shortest wave of the time series between 1970 and 1980, with a period of 2.5 years. For cluster 1 of July, the largest wave presents, from 1970 through 2010, a progressive change in frequency together with a frequency modulation effect. This period shows increasing wavelengths with time, reaching a 30-year period in 2010. Lower wavelengths were more variable, with an oscillation mode of period between 5 and 7 years from 1960 to 1990. A frequency change then occurred, giving rise to wavelengths of period about

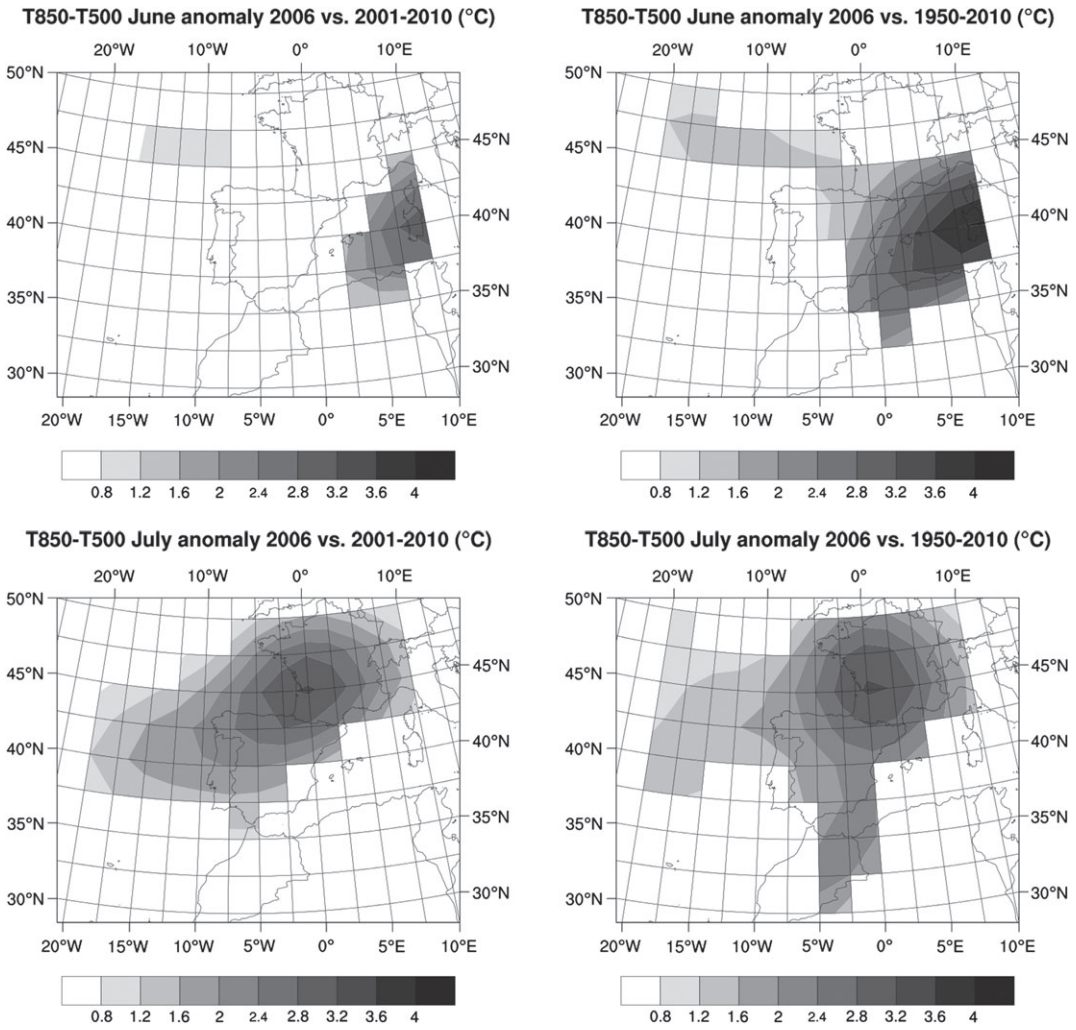

Figure 6. From left to right: Anomalies of temperature difference between 850 and 500 hPa of 2006, relative to 2001–2010 average and 1950–2010 average (top: June, bottom: July).

2.5 years, between 1990 and end of the signal. For cluster 2 in June, a wavelength of period about 27 years is distinguished for the first half of the signal. There was also a prevailing oscillation mode of period about 15–17 years over the full time series. As in the previous cases, higher frequency waves were also important for the series. It was possible to recognize the following for this wavelength range: one mode of period about 7.5 years, beginning in 1950 with frequency change around 1970, increasing the wavelength by 1–2 years, through 2010; another period about 2.5–3 years, which appeared suddenly during 1950 and 1990, lasting in both cases for 5 years. In cluster 2 of July, it is possible to decompose the signal into four wavelength ranges. The largest began in 1960 with a period of 27.5 years, with a frequency change between 1970 and 1980, persisting through the end with a period of about 22.5 years. Another structure from the initial time is a wave with a period of 10 years. A slight frequency modification is observable after 1980, decreasing the original wavelength to a period of 8 years. Another important range mode corresponds to a period of 6–7 years between 1950 and 1975, when a frequency change produced a wave around 3–4 years. Finally, the lower wavelength range corresponds to 2.5–3 years, which is perceptible throughout the study period.

4. Discussion and conclusions

The GFA has access to a complete database of all HD between May and September in the MEV since 2001. In June and July 2006, there were an exceptionally high number of hailstorms. Specifically, 33 HD were registered, 66% of hailstorms between May and September 2006 and 74% more than in June and July 2010, the year with the second highest number in these months. Using this information, characteristics of synoptic patterns in both months were studied, along with their differences with respect to 2001–2010 and 1950–2010.

The selected domain extends from 30°N to 50°N and 20°W to 10°E. Hailstorms are convective events so the selected atmospheric fields were temperature and geopotential height at 850 and 500 hPa, corresponding to gridded re-analysis data from the NCEP. Synoptic patterns

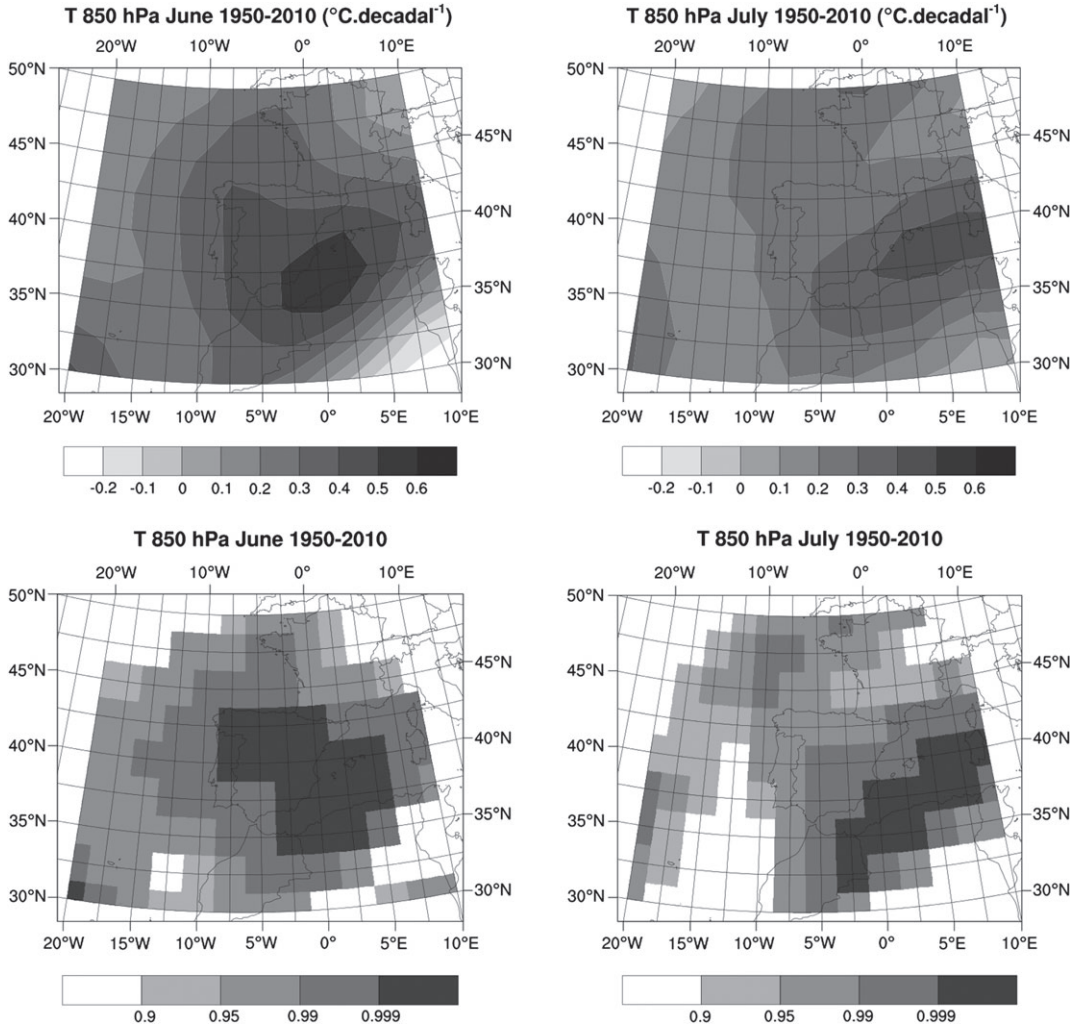

Figure 7. Top: Decadal rate of change of 850 hPa temperature over 1950–2010 in June (left) and July (right). Bottom: Level of significance $(1-\alpha)$.

of June and July 2006 show important differences in patterns relative to 2001–2010 and 1950–2010. Specifically, at 850 hPa, there was a deepening of the trough west of the IP, which extended to 500 hPa. This, along with reinforcement of high pressure centred over Algeria, generated a southerly component flow over north-east Spain.

Also in 2006, there were positive anomalies in the temperature difference at low and mid-tropospheric levels, owing to the temperature increase at 850 hPa. The anomalies, relative 2001–2010 reached 2.8–3.2 °C in June over Sardinia and 3.2–3.6 °C in July over southwest France. These anomalies deepened when calculated relative to 1950–2010, being 3.6–4.0 °C in June, and extending over the eastern coast of Spain in both months.

Trends of temperature and geopotential height at 850 hPa during 1950–2010 were studied. A positive trend was found for decadal rate of change in T850 over the IP. Maximum values were 0.5 °C per decade and 0.4 °C per decade in June and July, respectively, over the western Mediterranean, with level of significance $\alpha \leq 0.001$. The G850 also shows positive decadal rate of change in both months, with maximum values of 6 m per decade (June) and 5 m per decade (July) over the eastern study area.

These results show a change in atmospheric characteristics at 850 hPa between 1950 and 2010, implying a strengthening of the African ridge during this period. This evolution produced a positive trend of T850 in the area affected by the ridge, with maximum increase of 3 °C for T850 in June 1950–2010, over the western Mediterranean. This increase of T850 and deepening of the ridge generated winds with a strong southerly component over the MEV. This resulted in high water vapour contents and favourable environments for convective development and, specifically, an increase in the number of HD.

Once the trends and decadal rates of change in the selected fields were explored, periodicity of the T850 signal during 1950–2010 was analysed. Given the direct relationship between the results for T850 and G850, T850 was selected for the next stage of investigation. Previously, a CA for the T850 field was performed, using years as variables and grid points as cases for 1950–2010. The results show two very similar clusters for June and July. Cluster 1 includes the northern half and extreme

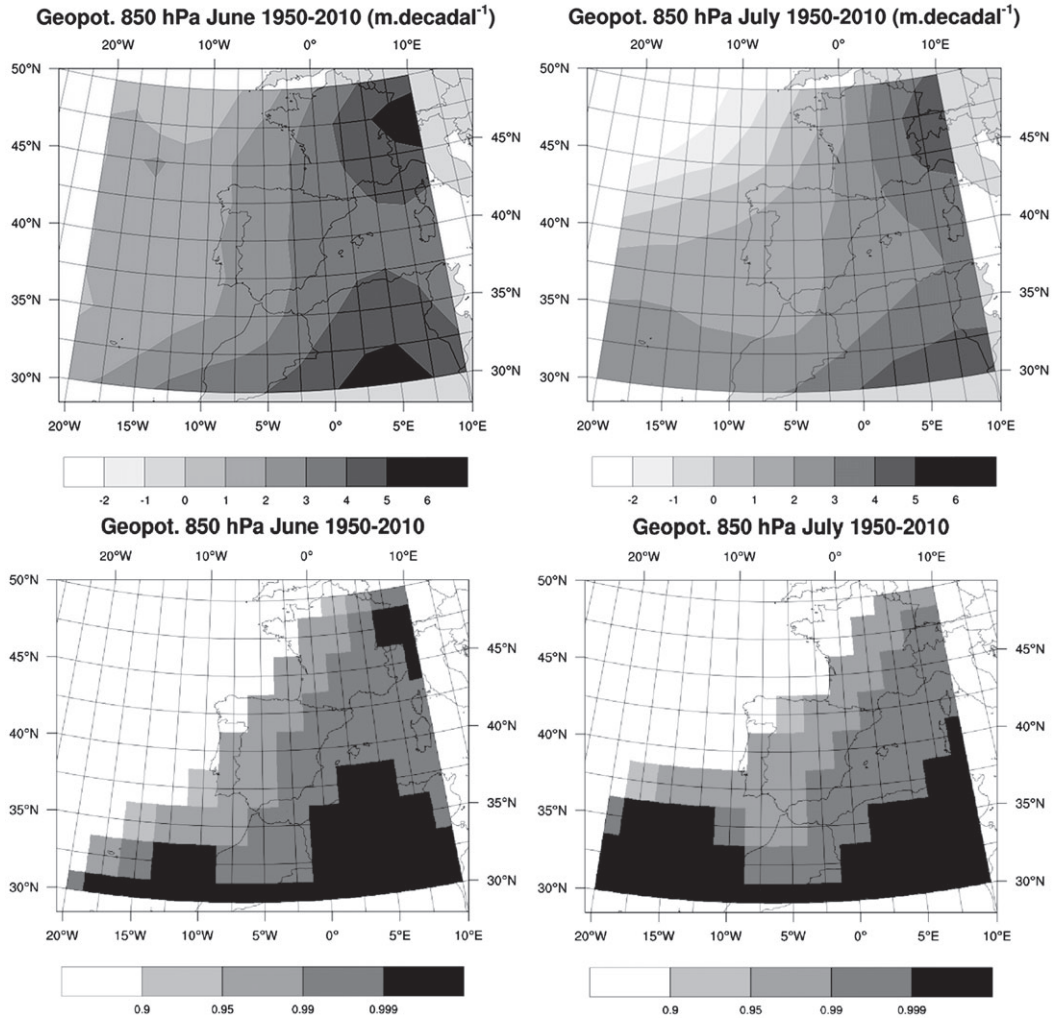

Figure 8. Top: Decadal rate of change of 850 hPa geopotential height over 1950–2010 in June (left) and July (right). Bottom: Level of significance $(1-\alpha)$.

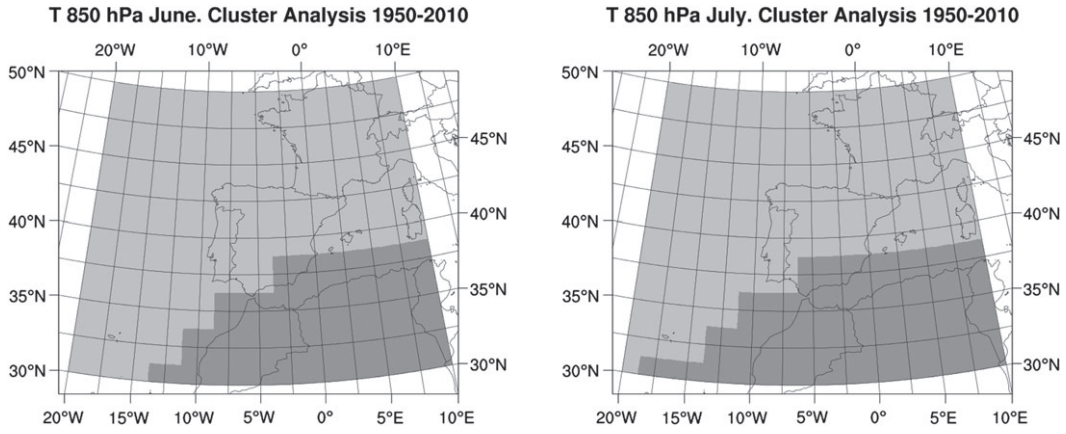

Figure 9. 850 hPa temperature clusters for 1950–2010 (left: June, right: July). Light grey colour is cluster 1 and dark grey is cluster 2.

southwest of the study domain, and cluster 2 the extreme south and southeast.

We obtained the periodicities of mean 850 hPa temperature during 1950–2010, applying CWT to each cluster of June and July. In cluster 2 for both months, there were a greater number of cycles. Generally, there was a small cycle of 2.5 years, which reached 3 years in cluster 2 for both months. In June, there was a larger cycle of 7 years in cluster 1 and of 7.5 years in cluster 2, changing to periods of 9–9.5 years, respectively. In July, these periodicities appeared smaller, generally beginning between 5 and 7 years and decreasing in both clusters.

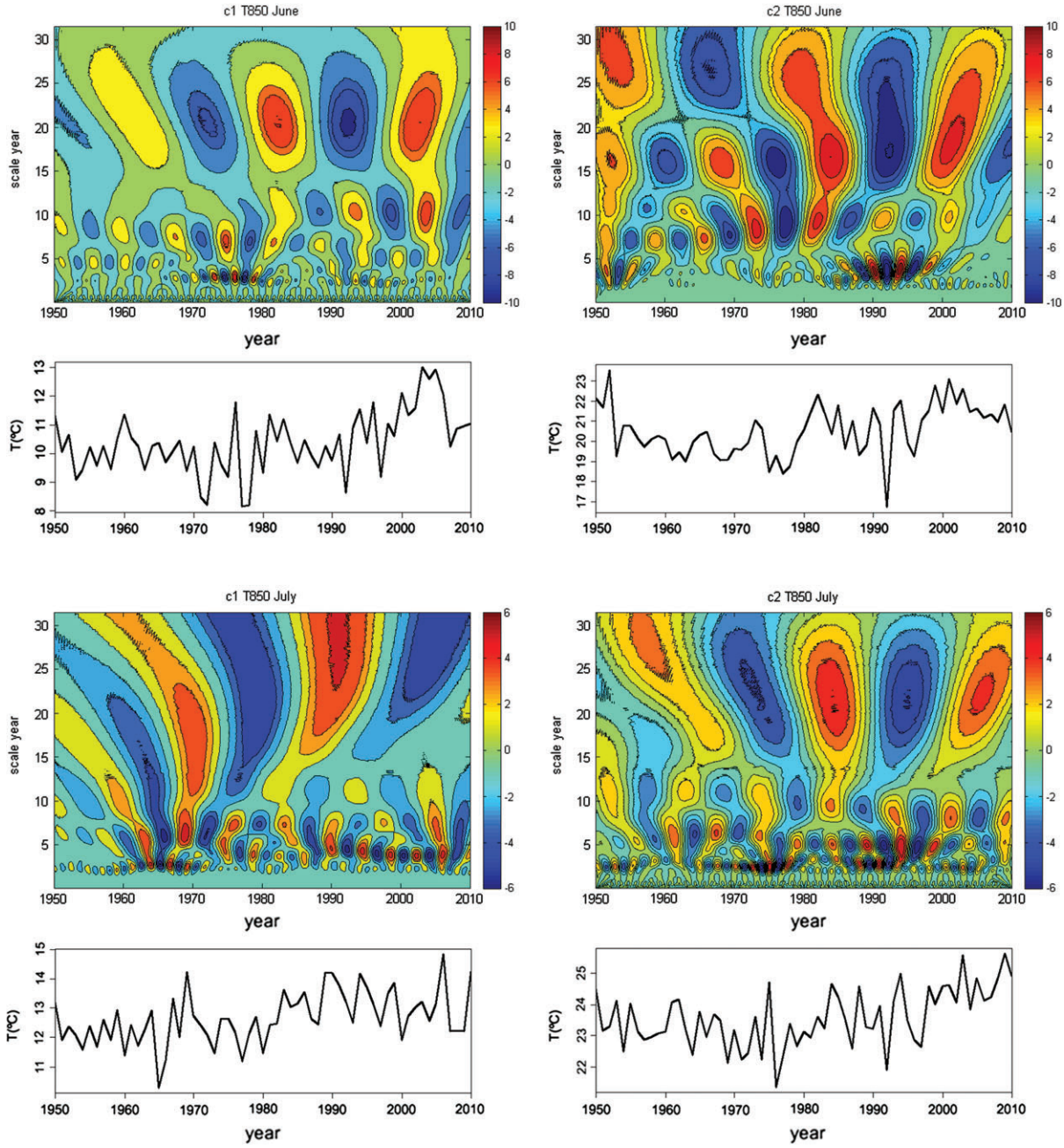

Figure 10. From left to right: Continuous wavelet power spectrum of detrended time series of 850 hPa temperature in June (top) and July (bottom) for clusters 1 and 2 and corresponding time series.

In cluster 2, there was a new periodicity of 15–17 years in June; in July, it was approximately 10 years and decreased to 8 years at the end of the series.

In all cases, greater periodicities were readily observed, except for cluster 1 in July. The periodicities varied from 20 years in cluster 1 of June to about 27 years in cluster 2. In cluster 2 of July, a cycle of 27.5 years decreased to 22.5 also in the half of the time series.

The anomaly of 2006 is also apparent in the time series of T850 (Figure 10). In cluster 1 of June, the CWT shows a possible effect of superposition of two cycles, which could be responsible for the high number of HD. This also occurred in 1980, though we do not have data from that year. One can detect the superposition of cycles in cluster 1 for July, although it is not observed with the same clarity, owing to the increase in high values of periodicity for this cluster.

The results show a clear change in temperature and geopotential fields at low tropospheric levels since 1950, affecting the western Mediterranean area. This change generates synoptic environments more favourable to development of hailstorms in north-east Spain, which increases the number of HD. Periodicities of mean 850 hPa temperature during 1950–2010 help explain the anomaly in 2006 and demonstrate the importance of more detailed analysis of periodicities in the temporal series.

Later studies will allow us to establish relationships between the periodicity and other factors, such as the NAO, solar radiation, solar activity or sunspot cycles, with subsequent improvement in the seasonal forecasting of hailstorms.

Acknowledgements

The study was supported by the Plan Nacional de I+D of Spain through grant CGL2010-15930 and the Junta de Castilla y León through grant LE176A11-2. The authors are grateful to Rocío Manjón for help with data processing.

References

Anderberg MR. 1973. *Cluster Analysis for Applications*. Academic Press: New York, NY; 359.

Beier CM, Signell SA, Luttman A, DeGaetano AT. 2012. High-resolution climate change mapping with gridded historical climate products. *Landsc. Ecol.* **27**: 327–342.

Berthet C, Dessens J, Sanchez JL. 2011. Regional and yearly variations of hail frequency and intensity in France. *Atmos. Res.* **100**: 391–400, DOI: 10.1016/j.atmosres.2010.10.008.

Botzen WJW, Bouwer LM, van den Bergh JCJM. 2010. Climate change and hailstorm damage: empirical evidence and implications for agriculture and insurance. *Resour. Energy Econ.* **32**: 341–362, DOI: 10.1016/j.reseneeco.2009.10.004.

Brooks HE, Lee JW, Craven JP. 2003. The spatial distribution of severe thunderstorm and tornado environments from global reanalysis data. *Atmos. Res.* **67–68**: 73–94, DOI: 10.1016/S0169-8095(03)00045-0.

Brooks HE, Dotzek N. 2008. The spatial distribution of severe convective storms and an analysis of their secular changes. In *Climate Extremes and Society*, Diaz HF, Murnane R (eds). Cambridge University Press: Cambridge, NY; 35–53.

Cao Z. 2008. Severe hail frequency over Ontario, Canada: recent trend and variability. *Geophys. Res. Lett.* **35**: L14803, DOI: 10.1029/2008GL034888.

Doswell CA III. 1987. The distinction between large-scale and mesoscale contribution to severe convection: a case study example. *Weather Forecast.* **2**: 3–16, DOI: 10.1175/1520-0434(1987)002<0003:TDBLSA>2.0.CO;2.

Farge M. 1992. Wavelet transforms and their applications to turbulence. *Annu. Rev. Fluid Mech.* **24**: 395–458, DOI: 10.1146/annurev.fl.24.010192.002143.

García-Ortega E, Fita L, Romero R, López L, Ramis C, Sánchez JL. 2007. Numerical simulation and sensitivity study of a severe hailstorm in northeast Spain. *Atmos. Res.* **83**: 225–241, DOI: 10.1016/j.atmosres.2005.08.004.

García-Ortega E, López L, Sánchez JL. 2011. Atmospheric patterns associated with hailstorm days in the Ebro Valley, Spain. *Atmos. Res.* **100**: 401–427, DOI: 10.1016/j.atmosres.2010.08.023.

García-Ortega E, Merino A, López L, Sánchez JL. 2012. Role of mesoscale factors at the onset of deep convection on hailstorm days and their relation to the synoptic patterns. *Atmos. Res.* **114–115**: 91–106, DOI: 10.1016/j.atmosres.2012.05.017.

Gong X, Richman MB. 1995. On the application of cluster analysis to growing season precipitation data in North America east of the Rockies. *J. Clim.* **8**: 897–931, DOI: 10.1175/1520-0442(1995)008<0897:OTAOCA>2.0.CO;2.

Heidinger H, Yarlequé C, Posadas A, Quiroz R. 2012. TRMM rainfall correction over the Andean Plateau using wavelet multi-resolution analysis. *Int. J. Remote Sens.* **33**(14): 4583–4602, DOI: 10.1080/01431161.2011.652315.

Houze R. 1993. *Cloud Dynamics*. Academic Press: San Diego, CA; 573.

IPCC. 2007. Climate Change 2007: synthesis report. In *Contribution of Working Groups I, II and III to the Fourth Assessment Report of the Intergovernmental Panel on Climate Change*, Core Writing Team, Pachauri RK, Reisinger A (eds). IPCC: Geneva, Switzerland; 104.

IPCC. 2012. Managing the risks of extreme events and disasters to advance climate change adaptation. In *A Special Report of Working Groups I and II of the Intergovernmental Panel on Climate Change*, Field CB, Barros V, Stocker TF, Qin D, Dokken DJ, Ebi KL, Mastrandrea MD, Mach KJ, Plattner G-K, Allen SK, Tignor M, Midgley PM (eds). Cambridge University Press: Cambridge, UK, and New York, NY; 582.

Kalnay E, Kanamitsu M, Kistler R, Collins W, Deaven D, Gandin L, Iredell M, Saha S, White G, Woollen J. 1996. The NCEP/NCAR 40-year reanalysis project. *Bull. Am. Meteorol. Soc.* **77**: 437–471, DOI: 10.1175/1520-0477(1996)077<0437:TNYRP>2.0.CO;2.

Kunz M, Sander J, Kottmeier C. 2009. Recent trends of thunderstorm and hailstorm frequency and their relation to atmospheric characteristics in southwest Germany. *Int. J. Climatol.* **29**: 2283–2297, DOI: 10.1002/joc.1865.

Labat D. 2005. Recent advances in wavelet analyses: part 1. A review of concepts. *J. Hydrol.* **314**: 275–288, DOI: 10.1016/j.jhydrol.2005.04.003.

Lau K, Weng H. 1995. Climate signal detection using wavelet transform: how to make a time series sing. *Bull. Am. Meteorol. Soc.* **76**: 2391–2402, DOI: 10.1175/1520-0477(1995)076<2391:CSDUWT>2.0.CO;2.

Leslie LM, Leplastrier M, Buckley BW. 2008. Estimating future trends in severe hailstorms over the Sydney Basin: a climate modelling study. *Atmos. Res.* **87**: 37–51, DOI: 10.1016/j.atmosres.2007.06.006.

Li M, Xia J, Chen Z, Meng D, Xu C. 2013. Variation analysis of precipitation during past 286 years in Beijing area, China, using non-parametric test and wavelet analysis. *Hydrol. Processes* **27**: 2934–2943, DOI: 10.1002/hyp.9388.

López L, Sánchez JL. 2009. Discriminant methods for radar detection of hail. *Atmos. Res.* **93**: 358–368, DOI: 10.1016/j.atmosres.2008.09.028.

Merino A, García-Ortega E, López L, Sánchez JL, Guerrero-Higueras AM. 2013. Synoptic environment, mesoscale configurations and forecast parameters for hailstorms in Southwestern Europe. *Atmos. Res.* **122**: 183–198, DOI: 0.1016/j.atmosres.2012.10.021.

Mohr S, Kunz M. 2013. Recent trends and variabilities of convective parameters relevant for hail events in Germany and Europe. *Atmos. Res.* **123**: 211–228, DOI: 10.1016/j.atmosres.2012.05.016.

Morlet J. 1983. *Sampling theory and wave propagation*. NATO ASI Series FI. Springer: Berlin; 233–261.

Niall S, Walsh K. 2005. The impact of climate change on hailstorms in Southeastern Australia. *Int. J. Climatol.* **25**: 1933–1952, DOI: 10.1002/joc.1233.

Partal T. 2012. Wavelet analysis and multi-scale characteristics of the runoff and precipitation series of the Aegean region (Turkey). *Int. J. Climatol.* **32**: 108–120.

Piani F, Crisci A, De Chiara G, Maracchi G, Meneguzzo F. 2005. Recent trends and climatic perspectives of hailstorms frequency and intensity in Tuscany and Central Italy. *Nat. Hazards Earth Syst. Sci.* **5**: 217–224, DOI: 10.5194/nhess-5-217-2005.

Saa A, García R, Díaz MC, Burgaz F, Tarquis M. 2011. Analysis of hail damages and temperature series for peninsular Spain. *Nat. Hazards Earth Syst. Sci.* **11**: 3415–3422, DOI: 10.5194/nhess-11-3415-2011, 2011.

Salmi T, Maatta A, Anttila P, Ruoho-Airola T, Amnell T. 2002. Detecting trends of annual values of atmospheric pollutants by the Mann–Kendall test and Sen's slope estimates – the excel template application MAKESENS. Report No. 31, Finnish Meteorological Institute. Helsinki, Finland, 35.

Sánchez JL, Gil-Robles B, Dessens J, Martin E, Lopez L, Marcos JL, Berthet C, Fernández JT, García-Ortega E. 2009. Characterization of hailstone size spectra in hailpads networks in France, Spain and Argentina. *Atmos. Res.* **93**: 641–654, DOI: 10.1016/j.atmosres.2008.09.033.

Sánchez JL, López L, García-Ortega E, Gil B. 2013. Nowcasting of kinetic energy of hail precipitation using radar. *Atmos. Res.* **123**: 48–60, DOI: 10.1016/j.atmosres.2012.07.021.

Sang Y. 2013. A review on the applications of wavelet transform in hydrology time series analysis. *Atmos. Res.* **122**: 8–15, DOI: 10.1016/j.atmosres.2012.11.003.

Schiesser H. 2003. Hagel. In *Extremereignisse und Klimaänderung. Organe consultatif sur les changements climatiques (OcCC)*, Bern, Switzerland, 65–68.

Sen PK. 1968. Estimates of the regression coefficient based on Kendall's tau. *J. Am. Stat. Assoc.* **63**: 1379–1389, DOI: 10.1080/01621459.1968.10480934.

Smith PL, Waldvogel A. 1989. On determinations of maximum hailstone sizes from hailpad observations. *J. Appl. Meteorol.* **28**: 71–76, DOI: 10.1175/1520-0450(1989)028<0071:ODOMHS>2.0.CO;2.

Tapiador FJ, Sánchez E. 2008. Changes in the European precipitation climatologies as derived by an ensemble of regional models. *J. Clim.* **21**: 2540–2557.

Tapiador FJ. 2010. A joint estimate of the precipitation climate signal in Europe using eight regional models and five observational datasets. *J. Clim.* **23**(7): 1719–1738, DOI: 10.1175/2009JCLI2956.1.

Tapiador FJ, Angelis CF, Viltard N, Cuartero F, de Castro M. 2011. On the suitability of regional climate models for reconstructing climatologies. *Atmos. Res.* **101**: 739–751, DOI: 10.1016/j.atmosres.2011.05.001.

Torrence C, Compo GP. 1998. A practical guide to wavelet analysis. *Bull. Am. Meteorol. Soc.* **79**: 61–78, DOI: 10.1175/1520-0477(1998)079<0061:APGTWA>2.0.CO;2.

TudurÍ E, Romero R, López L, García E, Sánchez JL, Ramis C. 2003. The 14 July 2001 hailstorm in northeastern Spain: diagnosis of the meteorological situation. *Atmos. Res.* **67–68**: 541–558.

Wang N, Lu C. 2010. Two-dimensional continuous wavelet analysis and its application to meteorological data. *J. Atmos. Oceanic Tech.* **27**: 652–666, DOI: 10.1175/2009JTECHA1338.1.

Xie B, Zhang Q, Wang Y. 2008. Trends in hail in China during 1960–2005. *Geophys. Res. Lett.* **35**: L13801.

Yi H, Shu H. 2012. The improvement of the Morlet wavelet for multi-period analysis of climate data. *C. R. Geosci.* **344**: 483–497, DOI: 10.1016/j.crte.2012.09.007.

